

# Towards Universal Certified Robustness with Multi-Norm Training

Enyi Jiang<sup>1</sup> David S. Cheung<sup>1</sup> Gagandeep Singh<sup>1</sup>

## Abstract

Existing certified training methods can only train models to be robust against a certain perturbation type (e.g.  $l_\infty$  or  $l_2$ ). However, an  $l_\infty$  certifiably robust model may not be certifiably robust against  $l_2$  perturbation (and vice versa) and also has low robustness against other perturbations (e.g. geometric and patch transformation). By constructing a theoretical framework to analyze and mitigate the tradeoff, we propose the first multi-norm certified training framework **CURE**, consisting of several multi-norm certified training methods, to attain better *union robustness* when training from scratch or fine-tuning a pre-trained certified model. Inspired by our theoretical findings, we devise bound alignment and connect natural training with certified training for better union robustness. Compared with SOTA-certified training, **CURE** improves union robustness to 32.0% on MNIST, 25.8% on CIFAR-10, and 10.6% on TinyImagenet across different epsilon values. It leads to better generalization on a diverse set of challenging unseen geometric and patch perturbations to 6.8% and 16.0% on CIFAR-10. Overall, our contributions pave a path towards *universal certified robustness*.

## 1. Introduction

Though deep neural networks (DNNs) are widely deployed in various vision applications, they remain vulnerable to adversarial attacks (Goodfellow et al., 2014; Kurakin et al., 2018). Though many empirical defenses (Madry et al., 2017; Zhang et al., 2019b; Wang et al., 2023) against adversarial attacks have been proposed, they do not provide provable guarantees and remain vulnerable to stronger attacks. Therefore, it is important to train DNNs to be *formally* robust against adversarial perturbations. Various works (Mirman et al., 2018; Gowal et al., 2018; Zhang et al., 2019a;

Balunović & Vechev, 2020; Shi et al., 2021; Müller et al., 2022a; Hu et al., 2023; 2024; Mao et al., 2024) on deterministic certified training against  $l_\infty$  and  $l_2$  perturbations have been proposed. However, those defenses are mostly limited to a certain type of perturbation and cannot easily be generalized to other perturbation types (Yang et al., 2022; Chiang et al., 2020). In Figure 1a, we show that an  $l_\infty$  certified robust model may lack  $l_2$  certified robustness and vice versa:  $l_\infty$  model only has 6.0%  $l_2$  robustness and  $l_2$  model has 0%  $l_\infty$  robustness. Multi-norm certified robustness is essential because this reflects real-world scenarios where adversaries can use multiple  $l_p$  perturbations. Also, Mangal et al. (2023) argues that  $l_p$  robustness is the bedrock for non- $l_p$  robustness. We also show that training with multi-norm robustness can lead to stronger *universal certified robustness* by generalizing better to other perturbation types such as geometric and patch transformations (Section 5.1).

To this end, we propose the first multi-norm Certified training for Union Robustness (**CURE**) framework, consisting of several multi-norm certified training methods. Inspired by SABR (Müller et al., 2022a), we use a deterministic  $l_2$  defense that first finds the  $l_2$  adversarial examples in a slightly truncated  $l_2$  region and then propagates the smaller  $l_\infty$  box using the IBP loss (Gowal et al., 2018). To effectively analyze the tradeoff between different  $l_p$  perturbations, we first construct a binary classification theoretical framework, from which we propose several baseline methods based on multi-norm empirical defenses with different loss formulations (Tramer & Boneh, 2019; Madaan et al., 2021; Croce & Hein, 2022; Jiang & Singh, 2024). Our proposed methods successfully improve union and universal certified robustness, shown in Table 2, Figure 3, and Table 3.

However, the aforementioned baseline methods achieve sub-optimal union robustness since they do not exploit the in-depth connections between certified training for different  $l_p$  perturbations as well as natural training. Inspired by the upper bound of theoretical analysis (Theorem 4.2), we propose a new *bound alignment* method to mitigate the  $l_q - l_r$  tradeoff better. Specifically, we regularize the distributions of output bound differences, computed with IBP, for  $l_q, l_r$  perturbations on the correctly certified subset  $\gamma$ , as shown in Figure 1b. In this way, we encourage the model to *emphasize optimizing* the samples that can potentially become certifiably robust against multi-norm perturbations. Specifically,

<sup>1</sup>Siebel School of Computing and Data Science, University of Illinois at Urbana-Champaign, Urbana, IL. Correspondence to: Enyi Jiang <enyij2@illinois.edu>.

we use a KL loss to encourage the distributions of the  $l_q, l_r$  output bound differences on subset  $\gamma$  to be close to each other for better union accuracy. Also, we find that there exist some useful components in natural training that can be extracted and leveraged to improve certified robustness (Jiang & Singh, 2024). To achieve this, we find and incorporate the layer-wise useful natural training components by comparing the similarity of the certified and natural training model updates. Lastly, fine-tuning an  $l_p$ -robust model using bound alignment quickly achieves superior multi-norm certified robustness. By addressing the  $l_q - l_r$  tradeoff, bound alignment preserves more  $l_q$  robustness when fine-tuning with  $l_r$  perturbations, focusing on correctly certified samples. This technique enables efficient multi-norm robustness using pre-trained models with single  $l_p$  robustness. Figure 1a shows that both scratch training (CURE-Scratch) and fine-tuning (CURE-Finetune) significantly enhance union robustness over single-norm training.

### Main Contributions:

- We design a theoretical framework to analyze multi-norm certified robustness tradeoff. Based on this, we propose three training methods CURE-Joint, CURE-Max, and CURE-Random with different loss formulations for better union and universal certified robustness.
- Inspired by our theoretical findings, we devise techniques including bound alignment, connecting natural training with certified training, and certified fine-tuning for better union robustness. CURE-Scratch and CURE-Finetune further facilitate the multi-norm certified training procedure and advance multi-norm robustness.
- Compared with SOTA certified training method (Müller et al., 2022a), **CURE** improves union robustness up to 32.0% on MNIST, 25.8% on CIFAR-10, and 10.6% on TinyImagenet. It improves robustness against diverse unseen geometric and patch perturbations up to 0.6%, 8.5% on MNIST and 6.8%, 16% on CIFAR-10 respectively, paving the way to universal certified robustness. Our code is available at <https://github.com/uiuc-focal-lab/CURE>.

## 2. Related Work

**Neural network verification.** We focus on deterministic verification methods, including abstract interpretation (Gehr et al., 2018; Singh et al., 2018; 2019a), optimization via linear programming (LP) (De Palma et al., 2021; Wang et al., 2021; Müller et al., 2022b), mixed integer linear programming (MILP) (Tjeng et al., 2017; Singh et al., 2019b), and semidefinite programming (SDP) (Raghunathan et al., 2018; Dathathri et al., 2020). These methods, often *incomplete*, trade precision for scalability as neural network verification is NP-complete (Katz et al., 2017). We analyze multi-norm certified training using deterministic verification techniques.

**Certified training.** For  $l_\infty$  certified training, IBP (Mirman et al., 2018; Gowal et al., 2018) minimizes a worst-case loss approximation using the Box relaxation method. CROWN-IBP (Zhang et al., 2019a) combines efficient Box propagation with precise linear relaxation bounds, while DeepZ (Wong et al., 2018; Singh et al., 2018) uses Cauchy random projections for relaxations. Balunović & Vechev (2020) propose a verifier-adversary framework, and Shi et al. (2021) enhance IBP with new weight initialization, batch normalization, and a warmup schedule. SABR (Müller et al., 2022a) and TAPS (Mao et al., 2024) improve IBP by linking it to adversarial training. Palma et al. (2024) achieves SOTA verified robustness via expressive losses. For  $l_2$  certified training, methods (Xu et al., 2022; Hu et al., 2023; 2024) use Lipschitz-based certification, although  $l_2$  robustness does not generalize to  $l_\infty$  perturbations. As shown in Table 9, our  $l_2$  defense outperforms Hu et al. (2023) on CIFAR-10. **CURE** is the first deterministic framework supporting multi-norm certified robustness across diverse architectures.

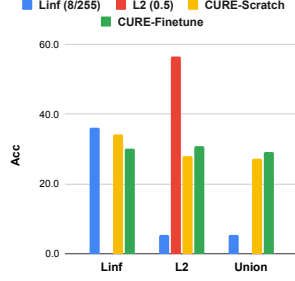
**Robustness against multiple perturbations.** Adversarial Training (AT) enhances robustness by using gradient descent to generate adversarial examples for training (Tramèr et al., 2017; Madry et al., 2017). Most methods focus on defending against a single perturbation type (Zhang et al., 2019b; Carmon et al., 2019; Raghunathan et al., 2020; Wang et al., 2020; Wu et al., 2020; Gowal et al., 2020; Zhang et al., 2021; Peng et al., 2023), leaving vulnerabilities to other perturbation types. Robustness to  $l_p$  attacks often fails to transfer to  $l_q$  attacks ( $q \neq p$ ) (Tramer & Boneh, 2019; Kang et al., 2019). Efforts to address multi-norm robustness include average-case (Tramer & Boneh, 2019), worst-case (Maini et al., 2020; Jiang & Singh, 2024), and random-sampled defenses (Madaan et al., 2021; Croce & Hein, 2022), as well as preprocessing, ensembles, and stability analyses (Nandy et al., 2020; Xiao et al., 2022). Probabilistic approaches like randomized smoothing (Nandi et al., 2023) improve certified multi-norm robustness but are computationally expensive. In contrast, our work introduces the first *deterministic* certified multi-norm training, achieving better multi-norm and universal certified robustness efficiently.

## 3. Background

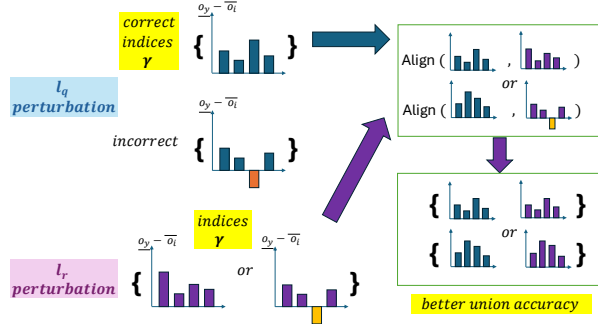
In this section, we provide the necessary background. Given samples  $\{(x_i, y_i)\}_{i=0}^N$  from a data distribution  $\mathcal{D}$ , the input comprises images  $x \in \mathbb{R}^d$  with labels  $y \in \mathbb{R}^k$ . The goal is to train a classifier  $f$ , parameterized by  $\theta$ , to minimize a loss function  $\mathcal{L} : \mathbb{R}^k \times \mathbb{R}^k \rightarrow \mathbb{R}$  over  $\mathcal{D}$ .

### 3.1. Neural network verification

Neural network verification formally proves a network’s robustness, with the provably robust samples defining the *certified accuracy*. Interval Bound Propagation (IBP) (Gowal et al., 2018; Mirman et al., 2018) is a simple yet effective



(a)  $l_\infty - l_2$  tradeoff on CIFAR10 with  $\epsilon_\infty = \frac{8}{255}$ ,  $\epsilon_2 = 0.5$ . The X-axis represents  $l_\infty$ ,  $l_2$ , and union robustness; different colors refer to different training methods.



(b) Bound alignment during training.

Figure 1: (a)  $l_\infty - l_2$  tradeoff: an  $l_\infty$  certified robust model may lack  $l_2$  certified robustness and vice versa. **CURE-Scratch** (yellow) and **CURE-Finetune** (green) improve union robustness significantly. (b) We align the output bound differences for  $l_q, l_r$  perturbations on the correctly certified  $l_q$  subset  $\gamma$  to mitigate  $l_q - l_r$  tradeoff for better union robustness.

method for verification. It over-approximates the input region  $B_p(x, \epsilon_p)$ ,  $p \in \{2, \infty\}$ , propagates it layer by layer through the network  $f = L_j \circ \sigma \circ L_{j-2} \circ \dots \circ L_1$  (with linear layers  $L_i$  and ReLU activations  $\sigma$ ), and verifies whether the reachable outputs classify correctly. Robustness is certified if the lower bound of the correct class exceeds the upper bounds of all others ( $\forall i \neq y, \bar{o}_i - \underline{o}_y < 0$ ).

### 3.2. Training for robustness

A classifier is adversarially robust on an  $l_p$ -norm ball  $B_p(x, \epsilon_p) = \{x' \in \mathbb{R}^d : \|x' - x\|_p \leq \epsilon_p\}$  if it correctly classifies all points within this region, i.e.,  $f(x') = y$  for all  $x' \in B_p(x, \epsilon_p)$ . The training for robustness is framed as a min-max optimization problem, defined for an  $l_p$  attack as:

$$\min_{\theta} \mathbb{E}_{(x, y) \sim \mathcal{D}} \left[ \max_{x' \in B_p(x, \epsilon_p)} \mathcal{L}(f(x'), y) \right] \quad (1)$$

The inner maximization problem cannot be solved exactly and is often approximated through adversarial training (Madry et al., 2017) or certified training (Gowal et al., 2018; Müller et al., 2022a). However, such methods are typically tailored to specific  $p$  values, leaving networks vulnerable to other perturbations. To address this, prior work has only trained networks to be *adversarially* robust against multiple perturbations ( $l_1, l_2, l_\infty$ ). Our focus is on training networks to be *certifiably* robust to multiple  $l_p$  perturbations.

### 3.3. Certified training

There are two main categories of methods to train certifiably robust models: unsound and sound methods. On the one hand, IBP, a sound method, optimizes the following loss function based on logit differences:

$$\mathcal{L}_{\text{IBP}}(x, y, \epsilon_\infty) = \ln(1 + \sum_{i \neq y} e^{\bar{o}_i - \underline{o}_y}) \quad (2)$$

On the other hand, the state-of-the-art certified training methods SABR (Müller et al., 2022a), TAPs (Mao et al., 2024) and Palma et al. (2024), sacrifice soundness to get a more precise approximation, resulting in better standard and certified accuracy. SABR finds an adversarial example  $x' \in B_\infty(x, \epsilon_\infty - \tau_\infty)$  and propagates a smaller box region  $B_\infty(x', \tau_\infty)$  using the IBP loss, which can be expressed as:

$$\mathcal{L}_{l_\infty}(x, y, \epsilon_\infty, \tau_\infty) = \max_{x' \in B_\infty(x, \epsilon_\infty - \tau_\infty)} \mathcal{L}_{\text{IBP}}(x', y, \tau_\infty) \quad (3)$$

### 3.4. Evaluation metrics

**Union certified accuracy.** We focus on the union threat model  $\Delta = B_1(x, \epsilon_1) \cup B_2(x, \epsilon_2) \cup B_\infty(x, \epsilon_\infty)$  which requires the DNN to be *certifiably* robust within the  $l_1, l_2$  and  $l_\infty$  adversarial regions simultaneously. Union accuracy is then defined as the robustness against  $\Delta_{(i)}$  for each  $x_i$  sampled from  $\mathcal{D}$ . In this paper, similar to the prior works (Croce & Hein, 2022), we use union accuracy as the main metric to evaluate the multi-norm *certified* robustness.

**Universal certified robustness.** We measure the generalization ability of multi-norm certified training to other perturbation types, including rotation, translation, scaling, shearing, contrast, and brightness change of geometric transformations (Balunovic et al., 2019; Yang et al., 2022), as well as patch attacks (Chiang et al., 2020). We define the average certified robustness across these adversaries as universal certified robustness.

## 4. CURE: multi-norm Certified training for Union Robustness

This section presents our multi-norm certified training framework **CURE**. First, for simplicity, we introduce a

theory framework using binary classification, to analyze the tradeoff between certified  $l_p$ ,  $l_q$  perturbations. However, we note our algorithms presented in this work are all multi-class and our theoretical framework can be extended to the multi-class case (Zhang et al., 2019b). Based on the theoretical analysis, we propose three baseline methods for multi-norm certified training against  $l_2$ ,  $l_\infty$  perturbations using different loss formulations, which serve as the base instantiations of our framework. Then, we design new techniques to improve union-certified accuracy inspired by our theoretical findings.

#### 4.1. Notations

For binary classification, we denote the sample instance as  $x \in \mathcal{X}$ , with the label  $y \in \{-1, +1\}$ , where  $\mathcal{X} \subseteq \mathbb{R}^d$  is the instance space. Let  $f : \mathcal{X} \rightarrow \mathbb{R}$  map instances to output values  $\in \{-1, +1\}$ , which can be parameterized (e.g., by deep neural networks). We use  $\mathbf{1}\{\text{event}\}$ , the 0-1 loss, as an indicator function that is 1 if an event happens and 0 otherwise. For any function  $\psi(u)$ , we use  $\psi^{-1}$  to denote the inverse function.  $\phi(\cdot)$  is commonly used to denote the surrogate for the 0-1 loss function.

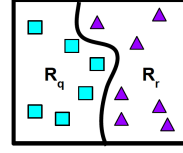
#### 4.2. Robust, boundary and union error

To characterize the robustness of a score function  $f : \mathcal{X} \rightarrow \mathbb{R}$ , similar to Schmidt et al. (2018); Cullina et al. (2018); Bubeck et al. (2019), we define *robust error* under the threat model of  $\epsilon_q$  perturbation:  $\mathcal{R}_q(f) := \mathbb{E}_{(x,y) \sim \mathcal{D}} \mathbf{1}\{\exists x'_q \in B_q(x, \epsilon_q) \text{ s.t. } f(x'_q)y \leq 0\}$ . Without the loss of generality, we define  $\mathcal{R}_r(f)$  similar to  $\mathcal{R}_q(f)$ , and assume  $\mathcal{R}_r(f) \geq \mathcal{R}_q(f)$ , which means  $l_r$  perturbation is generally stronger than the  $l_q$  one. Then, we introduce the *alignment error* as the risk calculated by  $x \in \mathcal{X}$  that are robust against  $l_r$  attack but not robust against  $l_q$  attack.  $\mathcal{R}_{\text{align}}(f) := \mathbb{E}_{(x,y) \sim \mathcal{D}} \mathbf{1}\{x'_r \in B_r(x, \epsilon_r), x'_q \in B_q(x, \epsilon_q), \text{ s.t. } f(x'_r)y > 0 \text{ and } f(x'_q)y \leq 0\}$ . Lastly, we define *union error* as the risk calculated by  $x \in \mathcal{X}$  either not robust against  $l_p$  or  $l_r$  attack. We have the following relationship of  $\mathcal{R}_{\text{union}}(f)$ :

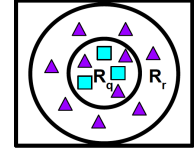
$$\mathcal{R}_{\text{union}}(f) = \mathcal{R}_r(f) + \mathcal{R}_{\text{align}}(f). \quad (4)$$

#### 4.3. Trade-off of $l_q$ , $l_r$ perturbations

Our study is motivated by the trade-off between  $l_q$  and  $l_r$  robust errors, as shown empirically in Figure 1a. To better illustrate the phenomenon, we provide an example with two extreme cases here. As shown in Table 1, we have (a) the *lowest* union accuracy of 0: when the instances that are not robust against  $l_q$ ,  $l_r$  are completely disjoint, we have a union error of 1; (b) the *highest* union accuracy of  $1 - \mathcal{R}_r$ : when the instances that are not robust against  $l_r$  attack includes all instances that are not robust against  $l_q$  attack, we have a union error  $\mathcal{R}_r$ . A larger union error indicates a bigger  $l_q$ ,  $l_r$  trade-off.  $\mathcal{R}_{\text{union}}$  is lower bounded by  $\mathcal{R}_r$ .



(a)  $\mathcal{R}_q$  and  $\mathcal{R}_r$  are disjoint



(b)  $\mathcal{R}_r$  includes  $\mathcal{R}_q$

Figure 2:  $l_q - l_r$  trade-off visualization. The large rectangle represents all input image instances. Blue and Purple points are instances belonging to  $\mathcal{R}_q$  and  $\mathcal{R}_r$ , respectively.

Table 1: Comparisons of union errors of two extreme cases. We notice  $\mathcal{R}_r \leq \mathcal{R}_{\text{union}} \leq 1$ . A larger union error demonstrates a more severe  $l_q - l_r$  trade-off.

	$\mathcal{R}_q$ and $\mathcal{R}_r$ are disjoint	$\mathcal{R}_r$ includes $\mathcal{R}_q$
$\mathcal{R}_{\text{align}}$	$1 - \mathcal{R}_q$	0
$\mathcal{R}_{\text{union}}$	1	$\mathcal{R}_r$ (optimal)

#### 4.4. Certified training for multiple norms

Eq. 4 reveals that we need to minimize  $\mathcal{R}_{\text{align}}$  by not only training with one kind of adversarial examples  $x'_r$  since it will lead to a large  $\mathcal{R}_{\text{align}}$  with more instances not robust against  $l_q$  attack. To effectively combine the optimization of  $l_q$  and  $l_r$  ( $q = 2, r = \infty$ ) certified training, based on the work (Tramer & Boneh, 2019; Madaan et al., 2021; Croce & Hein, 2022) on adversarial training for multiple norms, we propose the following methods:

1. **CURE-Joint**: optimizes  $\mathcal{L}_{l_\infty}$  and  $\mathcal{L}_{l_2}$  together:

$$\mathcal{L}_{\text{Joint}} = (1 - \alpha) \cdot \mathcal{L}_{l_\infty}(x, y, \epsilon_\infty, \tau_\infty) + \alpha \cdot \mathcal{L}_{l_2}(x, y, \epsilon_2, \tau_2)$$

It takes the sum of two worst-case IBP losses with  $l_\infty$  and  $l_2$  examples using a convex combination of weights with hyperparameter  $\alpha \in [0, 1]$ .

2. **CURE-Max**: compares  $\mathcal{L}_{l_2}$  and  $\mathcal{L}_{l_\infty}$ , selecting the higher IBP loss as the worse-case outcome. This approach acts as a *worst-case* defense, accounting for adversarial examples with the highest IBP loss across multiple perturbation types. The max loss  $\mathcal{L}_{\text{Max}}$  is defined as:

$$\mathcal{L}_{\text{Max}} = \max_{p \in \{2, \infty\}} \max_{x' \in B_p(x, \epsilon_p - \tau_p)} \mathcal{L}_{\text{IBP}}(x, y, \epsilon_p, \tau_p)$$

3. **CURE-Random**: randomly partitions a batch of data  $(\mathbf{x}, \mathbf{y}) \sim \mathcal{D}$  into equal sized blocks  $(\mathbf{x}_1, \mathbf{y}_1)$  and  $(\mathbf{x}_2, \mathbf{y}_2)$ . For  $(\mathbf{x}_1, \mathbf{y}_1)$ , we calculate the  $l_\infty$  worst-case IBP loss  $\mathcal{L}_{l_\infty}$  with  $l_\infty$  perturbations. For the other half  $(\mathbf{x}_2, \mathbf{y}_2)$ , similarly, we get the  $l_2$  worst-case IBP loss by applying  $l_2$  perturbations. After that, we optimize the **Joint** loss of these two with equal weights, as shown below. In this way, we reduce the time cost of propagating the bounds and generating the adversarial examples by  $\frac{1}{2}$ .

$$\mathcal{L}_{\text{Random}} = \mathcal{L}_{l_\infty}(\mathbf{x}_1, \mathbf{y}_2, \epsilon_\infty, \tau_\infty) + \mathcal{L}_{l_2}(\mathbf{x}_2, \mathbf{y}_2, \epsilon_2, \tau_2),$$

where  $\mathbf{x} = \mathbf{x}_1 \cup \mathbf{x}_2, \mathbf{y} = \mathbf{y}_1 \cup \mathbf{y}_2$



#### 4.5. Improved multi-norm certified training

The methods proposed above are still suboptimal as they fail to fully explore the relationship between worst-case IBP losses across different perturbations, certified training (CT), and natural training (NT). To address this, we introduce the following improvements to enhance the union robustness of **CURE**: (1) Inspired by our theory, we derive an upper bound on the terms, which informs us to propose a bound alignment technique to mitigate the trade-off better, improving multi-norm robustness. (2) We analyze and connect certified and natural training to attain better union accuracy. (3) the first certified fine-tuning method to quickly improve union accuracy with pre-trained single-norm models (Table 2).

##### 4.5.1. BOUND ALIGNMENT (BA)

First, we aim to design *tight* upper bounds for different risk terms, leveraging the theory of classification-calibrated loss, which informs how we design the technique to mitigate the  $l_r - l_q$  tradeoff better.

**Classification-calibrated surrogate loss** is a surrogate loss  $\mathcal{R}_\phi(f) := \mathbb{E}_{(x,y) \sim \mathcal{D}} \phi(f(x)y)$  designed to approximate the 0-1 loss, making it computationally efficient for optimization while maintaining a meaningful relationship with the true error (Zhang et al., 2019b). A loss is classification-calibrated if it ensures that any decision rule inconsistent with the Bayes optimal classifier has a strictly larger  $\phi$ -risk. This property is crucial for achieving optimal classification performance, and examples include hinge loss, logistic loss, and exponential loss. Here, we show the binary IBP loss falls into this loss category.

**Lemma 4.1.** *Binary IBP loss is a logistic loss in the classification-calibrated surrogate loss family.*

*Proof.* We have binary  $\mathcal{L}_{\text{IBP}}(x, y, \epsilon_p) = \ln(1 + e^{\bar{o}_i - \underline{o}_y})$ ,  $i \neq y$ , which is a logistic loss.

**Upper bound.** Our analysis provides a performance guarantee for minimizing the surrogate loss. Specifically, by Eq.4,  $\mathcal{R}_{\text{union}}(f) - \mathcal{R}_r^* = \mathcal{R}_r(f) - \mathcal{R}_r^* + \mathcal{R}_{\text{align}}(f) \leq \psi^{-1}(\mathcal{R}_\phi(f) - \mathcal{R}_\phi^*) + \mathcal{R}_{\text{align}}(f)$ , where the inequality holds as  $\phi$  is chosen to be a classification-calibrated loss (Bartlett et al., 2006) and  $\mathcal{R}_r^* := \min_f \mathcal{R}_r(f)$ . This yields the following result.

**Theorem 4.2.** *Let  $\mathcal{R}_\phi(f) := \mathbb{E} \phi(f(x)y)$  and  $\mathcal{R}_\phi^* := \min_f \mathcal{R}_\phi(f)$ . Under Assumption 1 in Zhang et al. (2019b), for any non-negative loss function  $\phi$  such that  $\phi(0) \geq 1$ , any measurable  $f : \mathcal{X} \rightarrow \mathbb{R}$ , any probability distribution on  $\mathcal{X} \times \{\pm 1\}$ , IBP output bound differences from  $f$  as  $d(x) = \bar{o}_i - \underline{o}_y$  ( $i \neq y$ ), and any  $\lambda > 0$ , we have*

$$\begin{aligned} \mathcal{R}_{\text{union}}(f) - \mathcal{R}_r^* &\leq \psi^{-1}(\mathcal{R}_\phi(f) - \mathcal{R}_\phi^*) \\ &+ \mathbb{E} \max_{\substack{x'_r \in B_r(x, \epsilon_r), \\ x'_q \in B_q(x, \epsilon_q)}} (\phi(d(x'_r)d(x'_q)/\lambda), \bar{o}_i \leq \underline{o}_y \text{ for } d(x'_r)). \end{aligned}$$

The proof is in Appendix A.1, which sheds light on how we can further improve union-certified robustness. Algorithmically, we can extend the framework to the case of multi-class classifications by replacing  $\phi$  with a multi-class calibrated loss  $L(\cdot, \cdot)$  (Zhang et al., 2019b).  $\phi(d(x'_r)d(x'_q)/\lambda)$  indicates that we need to *minimize the differences between output bounds of two perturbations* and  $\forall i \neq y, \bar{o}_i \leq \underline{o}_y$  means we need to regularize those bounds only on the *correctly predicted  $l_r$  subsets* (Definition 4.3), meaning the subset  $\gamma$  for which the lower bound computed with IBP of the correct class is higher than the upper bounds of other classes.

**Definition 4.3** (Correctly Certified  $l_r$  Subset). At epoch  $e$ , given the perturbation size  $\epsilon_r \in \mathbb{R}$  and model  $f$ , for a batch of data  $(\mathbf{x}, \mathbf{y}) \sim \mathcal{D}$  with size  $n$ , we have the output upper and lower bounds computed by IBP for  $l_r$  perturbations. We define a function  $h$  for this procedure as  $h(\mathbf{x}) = \{\bar{o}_j, \underline{o}_j\}_{j=0}^{j < n}$ , where  $\mathbf{o} = \{o_i\}_{i=0}^{i < k}$  is a vector of bounds for all classes. Then, the correctly certified subset  $\gamma$  at the current step is defined as:

$\forall j \in \gamma$  with  $(\mathbf{x}_j, \mathbf{y}_j)$  and bounds

$\{\bar{o}_j = \{\bar{o}_i\}_{i=0}^{i < k}, \underline{o}_j = \{\underline{o}_i\}_{i=0}^{i < k}\}$ , we have  $\forall i \neq y_j, \bar{o}_i \leq \underline{o}_{y_j}$ .

For certified training, people usually optimize the model using bound differences  $\{\bar{o}_i - \underline{o}_y\}_{i=0}^{i < k}$  ( $y$  is the correct class). Inspired by our theory, we align the bound differences  $\{\{\bar{o}_i - \underline{o}_y\}_{i=0, i \neq y}^{i < k}\}_n$  of  $l_r$  and  $l_q$  certified training outputs, specifically on the correctly certified  $l_q$  subset  $\gamma$ . Specifically, for each batch of data  $(\mathbf{x}, \mathbf{y}) \sim \mathcal{D}$ , we generate predicted bounds  $h(\mathbf{x}, q) = \{\bar{o}_{qj}, \underline{o}_{qj}\}_n$  and  $h(\mathbf{x}, r) = \{\bar{o}_{rj}, \underline{o}_{rj}\}_n$ . We denote their bounds differences after softmax normalization as  $d_q = \{\{\bar{o}_{qi} - \underline{o}_{qy}\}_{i=0, i \neq y}^{i < k}\}_n$  and  $d_r = \{\{\bar{o}_{ri} - \underline{o}_{ry}\}_{i=0, i \neq y}^{i < k}\}_n$ . Then, we select indices  $\gamma$ , according to Definition 4.3. We denote the size of the indices as  $n_c$ . We compute a KL-divergence loss over this set of samples using  $KL(d_q[\gamma] \| d_r[\gamma])$  (Eq. 5). Intuitively, we want to make  $d_r[\gamma]$  and  $d_q[\gamma]$  distributions close to each other, such that we gain more union robustness.

$$\mathcal{L}_{KL} = \frac{1}{n_c} \cdot \sum_{i=1}^{n_c} \sum_{j=0}^k d_q[\gamma[i]][j] \cdot \log \left( \frac{d_q[\gamma[i]][j]}{d_r[\gamma[i]][j]} \right) \quad (5)$$

Apart from the KL loss, we add another loss term using a Max-style approach in Eq. 6, since Max has relatively good performance, as shown in Table 2.  $\mathcal{L}_{Max}$  is the worst-case loss between  $l_r, l_q$  with the SABR loss. Our final loss  $\mathcal{L}_{\text{Scratch}}$  combines  $\mathcal{L}_{KL}$  and  $\mathcal{L}_{Max}$ , via a hyper-parameter  $\eta$ , as shown in Eq. 7.

$$\mathcal{L}_{Max} = \max_{p \in \{2, \infty\}} \max_{x' \in B_p(x, \epsilon_p - \tau_p)} \mathcal{L}_{\text{IBP}}(x, y, \epsilon_p, \tau_p) \quad (6)$$

$$\mathcal{L}_{\text{Scratch}} = \mathcal{L}_{Max} + \eta \cdot \mathcal{L}_{KL} \quad (7)$$

#### 4.6. Integrate NT into CT

In the context of adversarial robustness, [Jiang & Singh \(2024\)](#) shows that there exist some useful components in natural training, which can be extracted and properly integrated into adversarial training to get better adversarial robustness. We propose a technique to integrate NT into CT, to enhance union-certified robustness. Specifically, for model  $f^{(r)}$  at any epoch  $r$ , we examine the model updates of NT and CT over all samples from  $\mathcal{D}$ . The models  $f_n^{(r)}$  and  $f_c^{(r)}$  represent the results after one epoch of NT and CT, from the same initial model  $f^{(r)}$ . Then we compare the updates of the two  $g_n = f_n^{(r)} - f^{(r)}$  and  $g_c = f_c^{(r)} - f^{(r)}$ . For a specific layer  $l$ , by comparing  $g_n^l$  and  $g_c^l$ , we retain a portion of  $g_n^l$  according to their cosine similarity score (Eq.8). Negative scores indicate that  $g_n^l$  does not contribute to certified robustness, so we discard components with similarity scores  $\leq 0$ . The **GP** (Gradient Projection) operation, defined in Eq.9, projects  $g_c^l$  towards  $g_n^l$ .

$$\cos(g_n^l, g_c^l) = \frac{g_n^l \cdot g_c^l}{\|g_n^l\| \|g_c^l\|} \quad (8)$$

$$\mathbf{GP}(g_n^l, g_c^l) = \begin{cases} \cos(g_n^l, g_c^l) \cdot g_n^l, & \cos(g_n^l, g_c^l) > 0 \\ 0, & \cos(g_n^l, g_c^l) \leq 0 \end{cases} \quad (9)$$

Therefore, the total projected (useful) model updates  $g_p$  coming from  $g_n$  could be computed as Eq. 10. We use  $\mathcal{M}$  to represent all layers of the current model update. The expression  $\bigcup_{l \in \mathcal{M}}$  concatenates the useful natural model update components from all layers. A hyper-parameter  $\beta$  is introduced to balance the contributions of  $g_{GP}$  and  $g_c$ , as outlined in Eq.11. It is important to note that this projection procedure is applied only after the eps-annealing phase of certified training. The theoretical analysis of why connecting NT with CT works is discussed in Appendix A.2.

$$g_p = \bigcup_{l \in \mathcal{M}} \mathbf{GP}(g_n^l, g_c^l) \quad (10)$$

$$f^{(r+1)} = f^{(r)} + \beta \cdot g_p + (1 - \beta) \cdot g_c \quad (11)$$

##### 4.6.1. QUICK CERTIFIED FINE-TUNING

In practice, as the model architectures and datasets become larger, multi-norm certified training from scratch becomes more expensive. Also, there are many pre-trained models available with single norm certified training. In adversarial robustness, [Croce & Hein \(2022\)](#) shows it is possible to obtain state-of-the-art multi-norm robustness by fine-tuning a pre-trained model for a few epochs, which reduces the computational cost significantly. In this work, we propose the first fine-tuning certified multi-norm robustness scheme **CURE-Finetune**. Starting from a single norm pre-trained model, we perform the bound alignment technique by optimizing  $\mathcal{L}_{\text{Scratch}}$  for a few epochs. Because of the  $l_q - l_r$

tradeoff, certifiably finetuning a  $l_q$  pre-trained model on  $l_r$  perturbations reduces  $l_q$  robustness. Thus, we want to preserve more  $l_q$  robustness when doing certified fine-tuning, which makes bound alignment useful here. By regularizing on the correctly certified  $l_q$  subset with  $\mathcal{L}_{\text{Scratch}}$ , we can prevent losing more  $l_q$  robustness when boosting  $l_r$  robustness, which leads to better union accuracy. We note that **CURE-Finetune** can be adapted to any single-norm certifiably pre-trained models. As shown in Table 2, we can obtain a superior multi-norm certified robustness by performing fine-tuning on pre-trained  $l_\infty$  models for a few epochs.

## 5. Experiment

In this section, we present and discuss the results of union, geometric, and patch robustness, as well as ablation studies on hyper-parameters for MNIST, CIFAR-10, and TinyImageNet experiments. Other ablation studies, visualizations, and algorithms of **CURE** can be found in Appendix C and E.

**Experimental Setup.** For datasets, we use MNIST ([LeCun et al., 2010](#)) and CIFAR-10 ([Krizhevsky et al., 2009](#)) which both include 60K images with 50K and 10K images for training and testing, as well as TinyImageNet ([Le & Yang, 2015](#)) which consists of 200 object classes with 500 training images, 50 validation images, and 50 test images per class. We compare the following methods: 1.  $l_\infty$ : SOTA  $l_\infty$  certified defense SABR ([Müller et al., 2022a](#)), 2.  $l_2$ :  $l_2$  certified defense based on SABR, 3. **CURE-Joint**: take a weighted sum of  $l_2, l_\infty$  IBP losses. 4. **CURE-Max**: take the worst of  $l_2, l_\infty$  IBP losses. 5. **CURE-Random**: randomly partitions the samples into two blocks, then applies the Joint loss with equal weights. 6. **CURE-Scratch**: training from scratch with bound alignment and gradient projection techniques. 7. **CURE-Finetune**: robust fine-tuning with the bound alignment technique using  $l_\infty$  pre-trained models. We use a 7-layer convolutional architecture CNN7 similar to prior work ([Müller et al., 2022a](#)) for models. In Table 9, we compare our proposed  $l_2$  defense with [Hu et al. \(2023\)](#), where we show our method outperforms the SOTA  $l_2$  deterministic certified defense on CIFAR-10. We choose similar hyperparameters and training setup as [Müller et al. \(2022a\)](#) for  $l_\infty$  certified training. We select  $\alpha = 0.5$ ,  $l_2$  subselection ratio  $\lambda_2 = 1e^{-5}$ ,  $\beta = 0.5$ , and  $\eta = 2.0$  according to our ablation study results in Section 5.2 and Appendix C. For certified fine-tuning, we finetune 20% of the epochs from scratch. Full implementation details are in Appendix B. We find that SOTA single norm methods ([Mao et al., 2024](#); [Palma et al., 2024](#)) have bad union accuracy while we acknowledge that they can be extended to multi-norm training.

### 5.1. Main Results

**Evaluation.** We choose the common  $\epsilon_\infty, \epsilon_2, \epsilon_1$  values used in the literature ([Müller et al., 2022a](#); [Hu et al., 2023](#)) to construct multi-norm regions. These include ( $\epsilon_1 = 1.0, \epsilon_2 =$

Dataset	$(\epsilon_\infty, \epsilon_2, \epsilon_1)$	Methods	Clean	$l_\infty$	$l_2$	$l_1$	Union
MNIST	(0.1, 0.5, 1.0)	$l_\infty$	99.2	97.0	96.5	95.0	94.9
		$l_2$	99.5	2.6	98.6	98.0	2.6
		CURE-Joint	99.2	97.6	97.9	97.5	97.2
		CURE-Max	99.3	97.6	97.3	96.8	96.8
		CURE-Random	99.2	97.3	97.2	97.1	96.9
		CURE-Finetune	99.1	97.0	97.3	96.8	96.5
		CURE-Scratch	99.2	97.5	98.0	97.9	<b>97.5</b>
	(0.3, 1.0, 2.0)	$l_\infty$	98.7	92.1	69.6	38.9	38.5
		$l_2$	99.4	0.0	94.5	94.7	0.0
		CURE-Joint	98.7	90.5	76.3	50.8	50.3
		CURE-Max	98.7	91.1	76.2	47.2	46.5
		CURE-Random	98.7	90.5	76.3	50.8	50.3
		CURE-Finetune	98.5	90.1	83.5	64.0	63.2
		CURE-Scratch	98.0	89.4	85.9	71.5	<b>70.5</b>
	$(\frac{2}{255}, 0.25, 0.5)$	$l_\infty$	79.2	60.3	67.3	75.9	60.3
		$l_2$	82.1	5.8	71.3	81.7	5.8
		CURE-Joint	79.4	56.2	68.1	77.1	56.2
		CURE-Max	77.6	60.0	69.3	75.2	60.0
		CURE-Random	78.4	59.0	68.5	76.9	58.9
		CURE-Finetune	78.0	59.7	68.2	75.9	59.7
		CURE-Scratch	76.0	61.2	67.7	74.6	<b>61.2</b>
CIFAR-10	$(\frac{8}{255}, 0.5, 1.0)$	$l_\infty$	51.8	36.3	6.0	3.8	3.5
		$l_2$	78.6	0.0	56.5	75.8	0.0
		CURE-Joint	51.3	23.9	34.0	38.6	21.4
		CURE-Max	51.5	33.9	19.5	21.6	16.8
		CURE-Random	53.0	28.9	28.0	34.6	24.0
		CURE-Finetune	40.2	30.2	30.8	34.8	<b>29.3</b>
		CURE-Scratch	49.5	34.2	28.1	32.0	26.3
	$(\frac{1}{255}, \frac{36}{255}, \frac{72}{255})$	$l_\infty$	28.3	19.4	19.4	12.9	12.9
		$l_2$	36.2	2.9	30.6	23.5	2.9
		CURE-Joint	30.2	20.0	25.9	18.8	18.8
		CURE-Max	29.6	21.8	23.5	18.2	18.2
		CURE-Random	30.5	25.9	28.2	23.5	<b>23.5</b>
		CURE-Finetune	28.1	21.2	21.8	18.2	16.6
		CURE-Scratch	28.1	22.4	22.9	18.2	18.2

Table 2: Comparison of the clean accuracy, individual, and union certified accuracy (%) for different multi-norm certified training methods. **CURE** consistently improves union accuracy compared with single-norm training with significant margins on all datasets. **CURE-Scratch** and **CURE-Finetune** outperform other methods in most cases.

$0.5, \epsilon_\infty = 0.1$ ),  $(\epsilon_1 = 2.0, \epsilon_2 = 1.0, \epsilon_\infty = 0.3)$  for MNIST,  $(\epsilon_1 = 0.5, \epsilon_2 = 0.25, \epsilon_\infty = \frac{2}{255})$ ,  $(\epsilon_1 = 1.0, \epsilon_2 = 0.5, \epsilon_\infty = \frac{8}{255})$  for CIFAR-10 and  $(\epsilon_1 = \frac{72}{255}, \epsilon_2 = \frac{36}{255}, \epsilon_\infty = \frac{1}{255})$  for TinyImageNet. We make sure the adversarial regions with sizes  $\epsilon_\infty$ ,  $\epsilon_1$  and  $\epsilon_2$  do not include each other. We report the clean accuracy, certified accuracy against  $l_1, l_2, l_\infty$  perturbations, union accuracy, and individual/average certified robustness against geometric transformations as well as patch attacks. Further, we use alpha-beta crown (Zhang et al., 2018) for certification on  $l_2, l_\infty$  perturbations, FGV (Yang et al., 2022) for efficient certification of geometric transformations, and Chiang et al. (2020) for  $2 \times 2$  patch attacks.

**Union accuracy on MNIST, CIFAR-10, and TinyImageNet with CURE framework.** In Table 2, we show the results of clean accuracy and certified robustness against single and multi-norm with **CURE** on MNIST, CIFAR-10, and TinyImageNet. **CURE-Joint**, **CURE-Max**, and **CURE-Random** usually yield better union robustness than  $l_2$  and  $l_\infty$  certified training. Further, **CURE-Scratch** and **CURE-Finetune** consistently improve the union accuracy compared with other multi-norm methods with significant margins in most cases (20% for MNIST and 8% for CIFAR-10 experiments), showing the effectiveness of bound alignment and gradient projection techniques. Also, for quick fine-tuning, we show it is possible to quickly fine-tune a  $l_\infty$  robust model with good union robustness us-

Methods	MNIST	CIFAR-10
$l_\infty$	68.9	0.0
$l_2$	0.0	0.0
CURE-Joint	68.5	0.2
CURE-Max	65.8	0.1
CURE-Random	72.8	<b>16.0</b>
CURE-Scratch	<b>77.4</b>	10.1

Table 3: Robust accuracy against  $2 \times 2$  patch attacks on MNIST ( $\epsilon_1 = 2.0, \epsilon_2 = 1.0, \epsilon_\infty = 0.3$ ) and CIFAR-10 ( $\epsilon_1 = \frac{72}{255}, \epsilon_2 = \frac{36}{255}, \epsilon_\infty = \frac{1}{255}$ ) datasets. Results show **CURE** significantly outperforms single-norm training.

ing bound alignment, achieving SOTA union accuracy on MNIST ( $\epsilon_\infty = 0.3, \epsilon_2 = 1.0, \epsilon_1 = 2.0$ ) and CIFAR-10 ( $\epsilon_\infty = \frac{8}{255}, \epsilon_2 = 0.5, \epsilon_1 = 1.0$ ) experiments.

**Robustness against unseen geometric and patch transformations.** Table 3 and Table 6 (in Appendix) compares **CURE** with single norm training against various geometric perturbations on MNIST and CIFAR-10 datasets. **CURE** outperforms single norm training on diverse geometric transformations (0.6% for MNIST and 6% for CIFAR-10 on average), leading to better *universal certified robustness*. Also, **CURE-Scratch** has better geometric robustness than **CURE-Max** on both datasets, which reveals that bound alignment and gradient projection lead to better universal certified robustness. In addition, in Table 3, we display the certified robustness of **CURE** compared with single-norm baselines against patch  $2 \times 2$  attacks. Our framework outperforms related baselines with 8.5% for MNIST and 16.0% for CIFAR-10, showing better *universal certified robustness*.

## 5.2. Ablation Study

**Subselection ratio  $\lambda$ .** For  $l_\infty$  certified training, we use the same  $\lambda_\infty$  as in Müller et al. (2022a). For  $\lambda_2$ , in Figure 5a, we show the  $l_2$  certified robustness using varying  $\lambda_2 \in [1e^{-5}, 5e^{-5}, 5e^{-3}, 1e^{-2}]$  with  $\epsilon_2 = 0.5$ . Both clean and  $l_2$  accuracy improves when we have smaller  $\tau_2$  values. Based on the results, we choose  $\tau_2 = 1e^{-5}$  for our experiments.

**Bound alignment (BA) hyper-parameter  $\eta$ .** We perform CIFAR-10 ( $\epsilon_\infty = \frac{8}{255}, \epsilon_2 = 0.5, \epsilon_1 = 1.0$ ) experiments with  $\eta$  values in  $[0.5, 1.0, 1.5, 2.0, 4.0]$ . In Figure 5b, the clean accuracy generally drops as we have larger  $\eta$  values, with union accuracy improving then dropping. We pick  $\eta = 2.0$  with the best union accuracy for most experiments.

**Gradient projection (GP) hyper-parameter  $\beta$ .** Figure 5c displays the change of clean and union accuracy with choices of varying  $\beta$  values on CIFAR-10 ( $\epsilon_\infty = \frac{2}{255}, \epsilon_2 = 0.25, \epsilon_1 = 0.5$ ). **CURE-Scratch** is generally insensitive to  $\beta$  values. Thus, we choose  $\beta = 0.5$  for the experiments.

**Ablation study on BA and GP.** In Table 4, we show the ablation study of BA and GP techniques on the MNIST ( $\epsilon_\infty = 0.3, \epsilon_2 = 1.0, \epsilon_1 = 2.0$ ) experiment. BA and GP improve union accuracy by 5% and 24%, demonstrating the

Configs	R(30)	$T_u(2), T_v(2)$	Sc(5), R(5), C(5), B(0.01)	Sh(2), R(2), Sc(2), C(2), B(0.001)	Avg
$l_\infty$	54.6	20.9	82.5	95.6	63.4
$l_2$	0.0	0.0	0.0	0.0	0.0
CURE-Joint	<b>55.9</b>	21.3	82.3	<b>95.7</b>	63.8
CURE-Max	50.1	20.7	80.2	94.8	61.5
CURE-Random	54.8	18.8	83.5	95.6	63.2
CURE-Scratch	51.0	<b>24.3</b>	<b>85.5</b>	95.1	<b>64.0</b>

Figure 3: Comparison on **CURE** against geometric transformations for MNIST ( $\epsilon_1 = 2.0, \epsilon_2 = 1.0, \epsilon_\infty = 0.3$ ) experiment. We denote  $R(\varphi)$  a rotation of  $\pm\varphi$  degrees;  $T_u(\Delta u)$  and  $T_v(\Delta v)$  a translation of  $\pm\Delta u$  pixels horizontally and  $\pm\Delta v$  pixels vertically, respectively;  $Sc(\lambda)$  a scaling of  $\pm\lambda\%$ ;  $Sh(\gamma)$  a shearing of  $\pm\gamma\%$ ;  $C(\alpha)$  a contrast change of  $\pm\alpha\%$ ; and  $B(\beta)$  a brightness change of  $\pm\beta$ . **CURE** improves the geometric certified robustness compared with single norm training. Also, **CURE-Scratch** achieves the best average geometric transformation robustness.

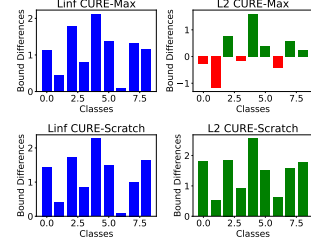
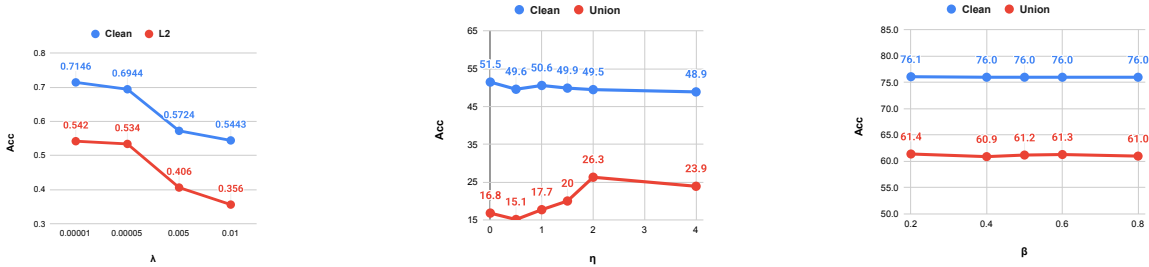


Figure 4: CURE-Max and CURE-Scratch bound difference visualization.



(a)  $\lambda_2$ : subselection ratio for  $l_2$ .

(b)  $\eta$ : weight for bound alignment.

(c)  $\beta$ : hyper-parameter for GP.

Figure 5: Ablation studies on  $\lambda_2$ ,  $\eta$  and  $\beta$  hyper-parameters.

	Clean	$l_\infty$	$l_2$	$l_1$	Union
CURE-Max	98.7	91.1	76.2	47.2	46.5
+BA	98.6	91.0	78.2	51.9	51.6
+BA + GP	98.0	89.4	85.9	71.5	<b>70.5</b>

Table 4: Ablations on BA and GP.

individual effectiveness of our proposed techniques.

**Visualization of bound differences.** Figure 4 displays the bound differences  $\{\phi_y - \bar{\phi}_i\}_{i=0, i \neq y}^{i < k}$  of one example that is improved by **CURE-Scratch** (second row), compared with the **CURE-Max** (first row), from the CIFAR-10 ( $\epsilon_\infty = \frac{8}{255}, \epsilon_2 = 0.5, \epsilon_1 = 1.0$ ) experiment. We use outputs from  $\alpha, \beta$ -CROWN. For  $l_2$  perturbations (blue diagrams), **CURE-Scratch** consistently shows positive bound differences enabling robust union prediction, while **CURE-Max** has several negative ones (highlighted in red). The second-row distributions are more aligned than the first, showing that **CURE-Scratch** effectively aligns bound differences. This highlights the effectiveness of the bound alignment method. Additional visualizations are in Appendix C.

### 5.3. Discussions

**Time cost of CURE.** The extra training costs of GP are small, taking 6, 24, 82 seconds using a single NVIDIA A40 GPU on MNIST, CIFAR-10, and TinyImageNet datasets (Table 11), respectively. Compared with the total training cost of **CURE-Scratch**, it only accounts for  $\sim 6\%$  of the

total cost. For runtime comparison of different methods, we have a complete runtime analysis (Table 10) in Appendix D for the MNIST experiment. We observe that **CURE-Joint** has the largest cost among all methods. **CURE-Scratch** has a small extra time cost than **CURE-Max**, showing the efficiency of our proposed techniques.

**Limitations.** For  $l_2$  certified training, we use a  $l_\infty$  box instead of  $l_2$  ball for bound propagation, which leads to more over-approximation and the potential loss of precision. Also, we notice drops in clean accuracy when training with **CURE** methods. In some cases, union accuracy improves slightly but clean accuracy and single  $l_p$  robustness reduce. BA and GP techniques lead to a slight decrease in clean accuracy in experiments.

## 6. Conclusion

We propose framework **CURE** with multi-norm certified training methods for better union robustness. We establish a theoretical framework to analyze the tradeoff between perturbations, which inspires us to devise bound alignment, gradient projection, and robust certified fine-tuning techniques, to enhance and facilitate the union-certified robustness. Extensive experiments on MNIST, CIFAR-10, and TinyImageNet show that **CURE** significantly improves union accuracy and robustness against geometric and patch transformations, paving the path to universal certified robustness.



## 7. Impact Statements

This paper presents work whose goal is to advance the field of Machine Learning. There are many potential societal consequences of our work, none which we feel must be specifically highlighted here.

## References

- Balunović, M. and Vechev, M. Adversarial training and provable defenses: Bridging the gap. In *8th International Conference on Learning Representations (ICLR 2020)(virtual)*. International Conference on Learning Representations, 2020.
- Balunovic, M., Baader, M., Singh, G., Gehr, T., and Vechev, M. Certifying geometric robustness of neural networks. *Advances in Neural Information Processing Systems*, 32, 2019.
- Bartlett, P. L., Jordan, M. I., and McAuliffe, J. D. Convexity, classification, and risk bounds. *Journal of the American Statistical Association*, 101(473):138–156, 2006.
- Bubeck, S., Lee, Y. T., Price, E., and Razenshteyn, I. Adversarial examples from computational constraints. In *International Conference on Machine Learning*, pp. 831–840. PMLR, 2019.
- Carmon, Y., Ragunathan, A., Schmidt, L., Duchi, J. C., and Liang, P. S. Unlabeled data improves adversarial robustness. *Advances in neural information processing systems*, 32, 2019.
- Chiang, P.-y., Ni, R., Abdelkader, A., Zhu, C., Studor, C., and Goldstein, T. Certified defenses for adversarial patches. In *International Conference on Learning Representations*, 2020. URL <https://openreview.net/forum?id=HyeaSkYYPH>.
- Croce, F. and Hein, M. Adversarial robustness against multiple and single  $l_p$ -threat models via quick fine-tuning of robust classifiers. In *International Conference on Machine Learning*, pp. 4436–4454. PMLR, 2022.
- Cullina, D., Bhagoji, A. N., and Mittal, P. Pac-learning in the presence of adversaries. *Advances in Neural Information Processing Systems*, 31, 2018.
- Dathathri, S., Dvijotham, K., Kurakin, A., Ragunathan, A., Uesato, J., Bunel, R. R., Shankar, S., Steinhardt, J., Goodfellow, I., Liang, P. S., et al. Enabling certification of verification-agnostic networks via memory-efficient semidefinite programming. *Advances in Neural Information Processing Systems*, 33:5318–5331, 2020.
- De Palma, A., Behl, H. S., Bunel, R., Torr, P., and Kumar, M. P. Scaling the convex barrier with active sets. In *Proceedings of the ICLR 2021 Conference*. Open Review, 2021.
- Gehr, T., Mirman, M., Drachler-Cohen, D., Tsankov, P., Chaudhuri, S., and Vechev, M. Ai2: Safety and robustness certification of neural networks with abstract interpretation. In *2018 IEEE symposium on security and privacy (SP)*, pp. 3–18. IEEE, 2018.
- Goodfellow, I. J., Shlens, J., and Szegedy, C. Explaining and harnessing adversarial examples. *arXiv preprint arXiv:1412.6572*, 2014.
- Gowal, S., Dvijotham, K., Stanforth, R., Bunel, R., Qin, C., Uesato, J., Arandjelovic, R., Mann, T., and Kohli, P. On the effectiveness of interval bound propagation for training verifiably robust models. *arXiv preprint arXiv:1810.12715*, 2018.
- Gowal, S., Qin, C., Uesato, J., Mann, T., and Kohli, P. Uncovering the limits of adversarial training against norm-bounded adversarial examples. *arXiv preprint arXiv:2010.03593*, 2020.
- Hu, K., Leino, K., Wang, Z., and Fredrikson, M. A recipe for improved certifiable robustness: Capacity and data. *arXiv preprint arXiv:2310.02513*, 2023.
- Hu, K., Zou, A., Wang, Z., Leino, K., and Fredrikson, M. Unlocking deterministic robustness certification on imagenet. *Advances in Neural Information Processing Systems*, 36, 2024.
- Jiang, E. and Singh, G. Ramp: Boosting adversarial robustness against multiple  $l_p$  perturbations. *arXiv preprint arXiv:2402.06827*, 2024.
- Kang, D., Sun, Y., Brown, T., Hendrycks, D., and Steinhardt, J. Transfer of adversarial robustness between perturbation types. *arXiv preprint arXiv:1905.01034*, 2019.
- Katz, G., Barrett, C., Dill, D. L., Julian, K., and Kochenderfer, M. J. Reluplex: An efficient smt solver for verifying deep neural networks. In *Computer Aided Verification: 29th International Conference, CAV 2017, Heidelberg, Germany, July 24-28, 2017, Proceedings, Part I 30*, pp. 97–117. Springer, 2017.
- Kim, H. Torchattacks: A pytorch repository for adversarial attacks. *arXiv preprint arXiv:2010.01950*, 2020.
- Kingma, D. P. Adam: A method for stochastic optimization. *arXiv preprint arXiv:1412.6980*, 2014.
- Krizhevsky, A., Hinton, G., et al. Learning multiple layers of features from tiny images. 2009.

- Kurakin, A., Goodfellow, I. J., and Bengio, S. Adversarial examples in the physical world. In *Artificial intelligence safety and security*, pp. 99–112. Chapman and Hall/CRC, 2018.
- Le, Y. and Yang, X. S. Tiny imagenet visual recognition challenge. 2015. URL <https://api.semanticscholar.org/CorpusID:16664790>.
- LeCun, Y., Cortes, C., and Burges, C. Mnist handwritten digit database. *ATT Labs [Online]*. Available: <http://yann.lecun.com/exdb/mnist>, 2, 2010.
- Madaan, D., Shin, J., and Hwang, S. J. Learning to generate noise for multi-attack robustness. In *International Conference on Machine Learning*, pp. 7279–7289. PMLR, 2021.
- Madry, A., Makelov, A., Schmidt, L., Tsipras, D., and Vladu, A. Towards deep learning models resistant to adversarial attacks. *arXiv preprint arXiv:1706.06083*, 2017.
- Maini, P., Wong, E., and Kolter, Z. Adversarial robustness against the union of multiple perturbation models. In *International Conference on Machine Learning*, pp. 6640–6650. PMLR, 2020.
- Mangal, R., Leino, K., Wang, Z., Hu, K., Yu, W., Pasareanu, C., Datta, A., and Fredrikson, M. Is certifying  $l_p$  robustness still worthwhile? *arXiv preprint arXiv:2310.09361*, 2023.
- Mao, Y., Müller, M., Fischer, M., and Vechev, M. Connecting certified and adversarial training. *Advances in Neural Information Processing Systems*, 36, 2024.
- Mirman, M., Gehr, T., and Vechev, M. Differentiable abstract interpretation for provably robust neural networks. In *International Conference on Machine Learning*, pp. 3578–3586. PMLR, 2018.
- Müller, M. N., Eckert, F., Fischer, M., and Vechev, M. Certified training: Small boxes are all you need. *arXiv preprint arXiv:2210.04871*, 2022a.
- Müller, M. N., Makarchuk, G., Singh, G., Püschel, M., and Vechev, M. Prima: general and precise neural network certification via scalable convex hull approximations. *Proceedings of the ACM on Programming Languages*, 6(POPL):1–33, 2022b.
- Nandi, S., Addepalli, S., Rangwani, H., and Babu, R. V. Certified adversarial robustness within multiple perturbation bounds. In *Proceedings of the IEEE/CVF Conference on Computer Vision and Pattern Recognition*, pp. 2298–2305, 2023.
- Nandy, J., Hsu, W., and Lee, M. L. Approximate manifold defense against multiple adversarial perturbations. In *2020 International Joint Conference on Neural Networks (IJCNN)*, pp. 1–8. IEEE, 2020.
- Palma, A. D., Bunel, R. R., Dvijotham, K. D., Kumar, M. P., Stanforth, R., and Lomuscio, A. Expressive losses for verified robustness via convex combinations. In *The Twelfth International Conference on Learning Representations*, 2024. URL <https://openreview.net/forum?id=mzyZ4wzKlM>.
- Peng, S., Xu, W., Cornelius, C., Hull, M., Li, K., Duggal, R., Phute, M., Martin, J., and Chau, D. H. Robust principles: Architectural design principles for adversarially robust cnns. *arXiv preprint arXiv:2308.16258*, 2023.
- Raghunathan, A., Steinhardt, J., and Liang, P. S. Semidefinite relaxations for certifying robustness to adversarial examples. *Advances in neural information processing systems*, 31, 2018.
- Raghunathan, A., Xie, S. M., Yang, F., Duchi, J., and Liang, P. Understanding and mitigating the tradeoff between robustness and accuracy. *arXiv preprint arXiv:2002.10716*, 2020.
- Schmidt, L., Santurkar, S., Tsipras, D., Talwar, K., and Madry, A. Adversarially robust generalization requires more data. *Advances in neural information processing systems*, 31, 2018.
- Shi, Z., Wang, Y., Zhang, H., Yi, J., and Hsieh, C.-J. Fast certified robust training with short warmup. *Advances in Neural Information Processing Systems*, 34:18335–18349, 2021.
- Singh, G., Gehr, T., Mirman, M., Püschel, M., and Vechev, M. Fast and effective robustness certification. *Advances in neural information processing systems*, 31, 2018.
- Singh, G., Gehr, T., Püschel, M., and Vechev, M. An abstract domain for certifying neural networks. *Proceedings of the ACM on Programming Languages*, 3(POPL):1–30, 2019a.
- Singh, G., Gehr, T., Püschel, M., and Vechev, M. Boosting robustness certification of neural networks. In *International conference on learning representations*, 2019b.
- Tjeng, V., Xiao, K., and Tedrake, R. Evaluating robustness of neural networks with mixed integer programming. *arXiv preprint arXiv:1711.07356*, 2017.
- Tramer, F. and Boneh, D. Adversarial training and robustness for multiple perturbations. *Advances in neural information processing systems*, 32, 2019.

- Tramèr, F., Kurakin, A., Papernot, N., Goodfellow, I., Boneh, D., and McDaniel, P. Ensemble adversarial training: Attacks and defenses. *arXiv preprint arXiv:1705.07204*, 2017.
- Wang, S., Zhang, H., Xu, K., Lin, X., Jana, S., Hsieh, C.-J., and Kolter, J. Z. Beta-crown: Efficient bound propagation with per-neuron split constraints for neural network robustness verification. *Advances in Neural Information Processing Systems*, 34:29909–29921, 2021.
- Wang, Y., Zou, D., Yi, J., Bailey, J., Ma, X., and Gu, Q. Improving adversarial robustness requires revisiting misclassified examples. In *ICLR*, 2020.
- Wang, Z., Pang, T., Du, C., Lin, M., Liu, W., and Yan, S. Better diffusion models further improve adversarial training. In Krause, A., Brunskill, E., Cho, K., Engelhardt, B., Sabato, S., and Scarlett, J. (eds.), *Proceedings of the 40th International Conference on Machine Learning*, volume 202 of *Proceedings of Machine Learning Research*, pp. 36246–36263. PMLR, 23–29 Jul 2023. URL <https://proceedings.mlr.press/v202/wang23ad.html>.
- Wong, E., Schmidt, F., Metzen, J. H., and Kolter, J. Z. Scaling provable adversarial defenses. *Advances in Neural Information Processing Systems*, 31, 2018.
- Wu, D., Xia, S.-T., and Wang, Y. Adversarial weight perturbation helps robust generalization. *Advances in Neural Information Processing Systems*, 33:2958–2969, 2020.
- Xiao, J., Qin, Z., Fan, Y., Wu, B., Wang, J., and Luo, Z.-Q. Adaptive smoothness-weighted adversarial training for multiple perturbations with its stability analysis. *arXiv preprint arXiv:2210.00557*, 2022.
- Xu, X., Li, L., and Li, B. Lot: Layer-wise orthogonal training on improving l2 certified robustness. *Advances in Neural Information Processing Systems*, 35:18904–18915, 2022.
- Yang, R., Laurel, J., Misailovic, S., and Singh, G. Provable defense against geometric transformations. *arXiv preprint arXiv:2207.11177*, 2022.
- Zhang, H., Weng, T.-W., Chen, P.-Y., Hsieh, C.-J., and Daniel, L. Efficient neural network robustness certification with general activation functions. *Advances in Neural Information Processing Systems*, 31:4939–4948, 2018. URL <https://arxiv.org/pdf/1811.00866.pdf>.
- Zhang, H., Chen, H., Xiao, C., Goyal, S., Stanforth, R., Li, B., Boning, D., and Hsieh, C.-J. Towards stable and efficient training of verifiably robust neural networks. *arXiv preprint arXiv:1906.06316*, 2019a.
- Zhang, H., Yu, Y., Jiao, J., Xing, E., El Ghaoui, L., and Jordan, M. Theoretically principled trade-off between robustness and accuracy. In *International conference on machine learning*, pp. 7472–7482. PMLR, 2019b.
- Zhang, J., Zhu, J., Niu, G., Han, B., Sugiyama, M., and Kankanhalli, M. Geometry-aware instance-reweighted adversarial training. In *International Conference on Learning Representations*, 2021. URL <https://openreview.net/forum?id=iAX016Cz8ub>.

## A. Proofs of the Theorems

In this section, we provide the proofs of the Theorems.

### A.1. Proof of Theorem 4.2

**Theorem 4.2 (restated).** Let  $\mathcal{R}_\phi(f) := \mathbb{E}\phi(f(x)y)$  and  $\mathcal{R}_\phi^* := \min_f \mathcal{R}_\phi(f)$ . Under Assumption 1 in Zhang et al. (2019b), for any non-negative loss function  $\phi$  such that  $\phi(0) \geq 1$ , any measurable  $f : \mathcal{X} \rightarrow \mathbb{R}$ , any probability distribution on  $\mathcal{X} \times \{\pm 1\}$ , IBP output bound differences from  $f$  as  $d(x) = \bar{o}_i - \underline{o}_y (i \neq y)$ , and any  $\lambda > 0$ , we have

$$\begin{aligned} \mathcal{R}_{\text{union}}(f) - \mathcal{R}_r^* &\leq \psi^{-1}(\mathcal{R}_\phi(f) - \mathcal{R}_\phi^*) + \Pr[x'_r \in B_r(x, \epsilon_r), x'_q \in B_q(x, \epsilon_q), f(x'_r)y > 0 \text{ and } f(x'_q)y \leq 0] \\ &\leq \psi^{-1}(\mathcal{R}_\phi(f) - \mathcal{R}_\phi^*) + \mathbb{E} \max_{\substack{x'_r \in B_r(x, \epsilon_r), \\ x'_q \in B_q(x, \epsilon_q)}} (\phi(f(x'_r)f(x'_q)/\lambda), f(x'_r)y > 0) \\ &\leq \psi^{-1}(\mathcal{R}_\phi(f) - \mathcal{R}_\phi^*) + \mathbb{E} \max_{\substack{x'_r \in B_r(x, \epsilon_r), \\ x'_q \in B_q(x, \epsilon_q)}} (\phi(d(x'_r)d(x'_q)/\lambda), \bar{o}_i \leq \underline{o}_y \text{ for } d(x'_r)). \end{aligned}$$

*Proof.* By Eqn. equation 4,  $\mathcal{R}_{\text{union}}(f) - \mathcal{R}_r^* = \mathcal{R}_r(f) - \mathcal{R}_r^* + \mathcal{R}_{\text{align}}(f) \leq \psi^{-1}(\mathcal{R}_\phi(f) - \mathcal{R}_\phi^*) + \mathcal{R}_{\text{align}}(f)$ , where the last inequality holds because we choose  $\phi$  as a classification-calibrated loss (Bartlett et al., 2006). This leads to the first inequality.

Also, notice that

$$\begin{aligned} &\Pr[x'_r \in B_r(x, \epsilon_r), x'_q \in B_q(x, \epsilon_q), f(x'_r)y > 0 \text{ and } f(x'_q)y \leq 0] \\ &\leq \Pr[x'_r \in B_r(x, \epsilon_r), x'_q \in B_q(x, \epsilon_q), f(x'_r)f(x'_q) \leq 0, f(x'_r)y > 0] \\ &= \mathbb{E} \max_{\substack{x'_r \in B_r(x, \epsilon_r), \\ x'_q \in B_q(x, \epsilon_q)}} (\mathbf{1}\{f(x'_r) \neq f(x'_q)\}, f(x'_r)y > 0) \\ &= \mathbb{E} \max_{\substack{x'_r \in B_r(x, \epsilon_r), \\ x'_q \in B_q(x, \epsilon_q)}} (\mathbf{1}\{f(x'_r)f(x'_q)/\lambda < 0\}, f(x'_r)y > 0) \\ &\leq \mathbb{E} \max_{\substack{x'_r \in B_r(x, \epsilon_r), \\ x'_q \in B_q(x, \epsilon_q)}} (\phi(f(x'_r)f(x'_q)/\lambda), f(x'_r)y > 0) \\ &\leq \mathbb{E} \max_{\substack{x'_r \in B_r(x, \epsilon_r), \\ x'_q \in B_q(x, \epsilon_q)}} (\phi(d(x'_r)d(x'_q)/\lambda), \bar{o}_i \leq \underline{o}_y \text{ for } d(x'_r)). \end{aligned}$$

The last inequality holds because the adversarial loss is always upper-bounded by the IBP loss. Therefore, we get the second and third inequality in Theorem A.1.  $\square$

### A.2. Theory of connecting NT with CT

The proof for connecting NT with CT via gradient projection (GP) is very similar to what has been done in Jiang & Singh (2024), where authors analyze and compare the delta errors of two aggregation rules (standard training and training with GP). Delta errors are the indicators of convergences of different aggregation rules based on a mild assumption on the Lipschitz continuity of loss function gradients. GP leads to a smaller Delta error, which means GP results in a better convergence. The only difference in connecting NT with CT is that we use a different loss function compared with adversarial training, which makes the proof almost the same. One can refer to Jiang & Singh (2024) for the more detailed proof of GP.

## B. More training details

**Certified training for  $l_2$  robustness.** We propose a new deterministic certified training method against  $l_2$  adversarial perturbations, inspired by SABR (Müller et al., 2022a). For the specified  $\epsilon_2$  and  $\tau_2$  values for  $l_2$  certified training, we first search for the  $l_2$  adversarial examples using standard  $l_2$  adversarial attacks (Kim, 2020)  $x' \in B_2(x, \epsilon_2 - \tau_2)$  in the slightly truncated  $l_2$  ball. After that, we propagate a smaller box region  $B_\infty(x', \tau_2)$  using the IBP loss. The loss we optimize can be formulated as follows:



$$\mathcal{L}_{l_2}(x, y, \epsilon_2, \tau_2) = \max_{x' \in B_2(x, \epsilon_2 - \tau_2)} \mathcal{L}_{\text{IBP}}(x', y, \tau_2)$$

**Training details.** We mostly follow the hyper-parameter choices from Müller et al. (2022a) for CURE. We include weight initialization and warm-up regularization from Shi et al. (2021). Further, we use ADAM (Kingma, 2014) with an initial learning rate of  $1e^{-4}$ , decayed twice with a factor of 0.2. For CIFAR-10, we train 160 and 180 epochs for  $(\epsilon_\infty = \frac{2}{255}, \epsilon_2 = 0.25)$  and  $(\epsilon_\infty = \frac{8}{255}, \epsilon_2 = 0.5)$ , respectively. We decay the learning rate after 120 and 140, 140 and 160 epochs, respectively. For the TinyImagenet experiment, we use the same setting as the CIFAR-10  $(\epsilon_\infty = \frac{8}{255}, \epsilon_2 = 0.5)$  experiment. For the MNIST dataset, we train 70 epochs, decaying the learning rate after 50 and 60 epochs. For batch size, we set 128 for CIFAR-10 and TinyImagenet and 256 for MNIST. For all experiments, we first perform one epoch of standard training. Also, we anneal  $\epsilon_\infty, \epsilon_2$  from 0 to their final values with 80 epochs for CIFAR-10 and TinyImagenet and 20 epochs for MNIST. We only apply GP after training with the final epsilon values. For certification, we verify 1000 examples on MNIST and CIFAR-10, as well as 170 examples on TinyImagenet. The values of all hyperparameters can be found in Table 5.

	MNIST-small	MNIST-large	CIFAR-small	CIFAR-large	TinyImagenet
$\lambda_\infty$	0.4	0.6	0.1	0.7	0.4
$\lambda_2$	1.00E-05	1.00E-05	1.00E-05	1.00E-05	1.00E-05
Learning rate	1.00E-04	1.00E-04	1.00E-04	1.00E-04	1.00E-04
LR decay ratio	0.2	0.2	0.2	0.2	0.2
Training epochs	70	70	160	180	180
Decay epochs	50, 60	50, 60	120, 140	140, 160	140, 160
Batch size	256	256	128	128	128
$\alpha$ (CURE)	0.5	0.5	0.5	0.5	0.5
$\eta$ (CURE)	2.0	0.5	2.0	2.0	2.0
$\beta$ (CURE)	0.5	0.5	0.5	0.5	0.5

Table 5: Training specifications of our main experiments on MNIST, CIFAR-10, and TinyImagenet.

**Certifications for evaluations on  $l_1, l_2, l_\infty$  norms.** We evaluated our trained models using  $\alpha, \beta$ -CROWN (Zhang et al., 2018). Specifically,  $\alpha, \beta$ -CROWN employs an efficient linear bound propagation framework coupled with a branch-and-bound algorithm to certify the robustness of neural networks against adversarial attacks. It propagates bounds on network outputs layer-by-layer. These bounds are linear functions representing the range of potential values the network’s output can take under a given set of input constraints. In addition, the branch-and-bound algorithm systematically divides the input space into smaller regions (branching) and computes tighter bounds on each subregion.  $\alpha, \beta$ -CROWN is versatile and supports various activation functions, including ReLU, sigmoid, and tanh, making it applicable to a wide range of neural network architectures. Also, it supports the certification on different  $l_p$  ( $p = 1, 2, \infty$ ) norms, which fits the goal of our CURE framework for multi-norm certified robustness.

## C. Other experiment results and ablation studies

**Robustness against geometric transformations on CIFAR-10.** Table 6 displays the certified robustness against geometric transformations on CIFAR-10. CURE outperforms the single-norm baselines with significant margins. Also, we notice that CURE-Scratch improves CURE-Max, which indicates the effectiveness of bound alignment and gradient projection.

**Comparison of  $l_2$  certified training and PGD training.** Table 7 shows the  $l_2$  certified robustness comparison between certified training and PGD training. The results demonstrate that determinist-certified training greatly improves the certified robustness.

**Hyper-parameter  $\alpha$  for Joint certified training.** As shown in Table 8, we test the changing of  $l_\infty, l_2$ , and union accuracy with different  $\alpha$  values in  $[0, 0.25, 0.5, 0.75, 1.0]$  on MNIST  $(\epsilon_\infty = 0.1, \epsilon_2 = 0.5)$  experiments. We observe that  $\alpha = 0.5$  has the best union accuracy and is generally a good choice for our experiments by balancing the two losses.

**Comparison of  $l_2$  certified robustness on  $l_2$  deterministic certified training methods.** In Table 9, we compare our proposed  $l_2$  certified defense with SOTA  $l_2$  certified defense Hu et al. (2023) on CIFAR-10 with  $\epsilon_2 = 0.25$  and 0.5. The

Confgs	R(10)	R(2),Sh(2)	Sc(1),R(1), C(1),B(0.001)	Avg
$l_\infty$	27.8	33.2	23.3	28.1
$l_2$	36.6	0.0	0.0	12.2
CURE-Joint	<b>35.0</b>	<b>41.4</b>	<b>28.2</b>	<b>34.9</b>
CURE-Max	33.7	39.0	23.3	32.0
CURE-Random	35.1	40.9	26.2	34.1
CURE-Scratch	34.2	39.6	24.9	32.9

Table 6: Comparison on **CURE** against geometric transformations for CIFAR-10 experiment. **CURE** improves the universal certified robustness significantly compared with single norm training.

$l_2$ certified robustness	MNIST-large	CIFAR-small	CIFAR-large
Certified training	<b>94.5</b>	<b>71.2</b>	<b>56.6</b>
PGD training	74.3	23.3	10.2

Table 7: Comparison on  $l_2$  certified robustness between certified and PGD training.

$\alpha$	0.0	0.25	0.5	0.75	1.0
Clean	99.2	99.2	99.3	99.2	99.5
$l_\infty$	97.7	97.7	97.5	97.2	2.0
$l_2$	96.9	95.6	97.4	95.9	98.7
Union	96.9	95.6	<b>97.1</b>	95.8	2.0

Table 8: Ablation study on Joint training hyper-parameter  $\alpha$ .

results show that our proposed  $l_2$  deterministic certified training method improves over  $l_2$  robustness by  $2 \sim 4\%$  compared with the SOTA method.

$\epsilon_2$	0.25	0.5
<a href="#">Hu et al. (2023)</a>	69.5	52.2
Ours	<b>71.2</b>	<b>56.6</b>

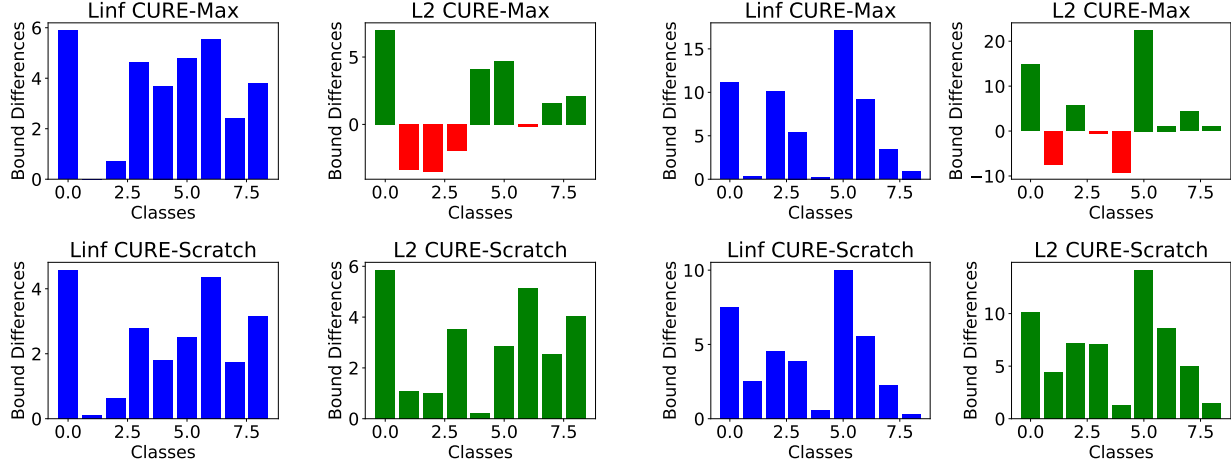
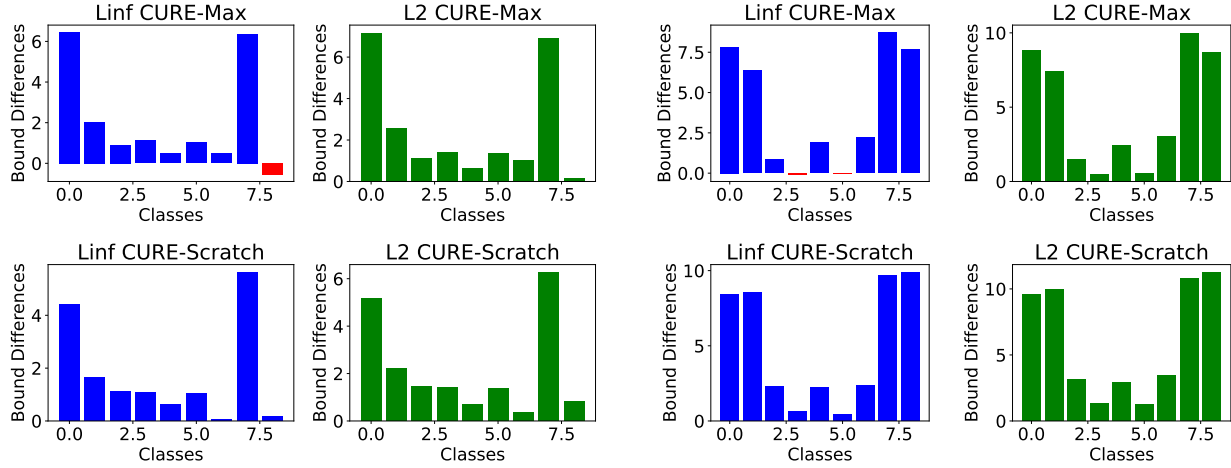
Table 9: Comparison of  $l_2$  certified accuracy: our proposed  $l_2$  certified training consistently outperforms [Hu et al. \(2023\)](#) by  $2 \sim 4\%$ .

**More visualizations on bound differences.** We plot the bound difference examples from alpha-beta-crown on MNIST, CIFAR-10, and TinyImagenet datasets, where the negative bound differences are colored in red. As shown in Figure 6, 7, 8, we compare CURE-Scratch (second row) with CURE-Max (first row), with bound differences against  $l_\infty$  and  $l_2$  perturbations colored in blue and green, respectively. CURE-Scratch produces all positive bound differences, leading to unionly robust predictions; CURE-Max is not unionly robust due to some negative bound differences. Also, we observe that CURE-Scratch successfully brings  $l_q, l_r$  bound difference distributions close to each other compared with CURE-Max in many cases, which confirms the effectiveness of our bound alignment technique.

## D. Runtime Analysis

This section provides the runtime per training epoch for all methods on MNIST ( $\epsilon_\infty = 0.1, \epsilon_2 = 0.75$ ) experiments and runtime per training epoch of CURE-Scratch with ablation studies on GP for MNIST, CIFAR10, and TinyImagenet experiments. We evaluate all the methods on a single A40 Nvidia GPU with 40GB memory and the runtime is reported in seconds (s).

**Runtime for different methods on MNIST experiments.** In Table 10, we show the time in seconds (s) per training epoch for single norm training ( $l_\infty$  and  $l_2$ ), CURE-Joint, CURE-Max, CURE-Random, CURE-Scratch, and CURE-Finetune methods. CURE-Finetune has a relatively small training cost compared with other methods and CURE-Joint has the

Figure 6: Bound difference visualizations on MNIST ( $\epsilon_\infty = 0.3, \epsilon_2 = 1.0$ ) experiments.Figure 7: Bound difference visualizations on CIFAR-10 ( $\epsilon_\infty = \frac{2}{255}, \epsilon_2 = 0.25$ ) experiments.

highest time cost (around two times of other methods) per epoch. The results indicate the efficiency of training with CURE-Scratch/Finetune.

Methods	Runtime (s)
$l_\infty$	89
$l_2$	82
CURE-Joint	155
CURE-Max	147
CURE-Random	101
CURE-Finetune	148
CURE-Scratch	153

Table 10: Runtime for all methods on MNIST ( $\epsilon_\infty = 0.1, \epsilon_2 = 0.5$ ) experiment per epoch in seconds.

**Runtime for CURE-Scratch on MNIST, CIFAR10, and TinyImagenet datasets.** In Table 11, we show the runtime per training epoch using CURE-Scratch on MNIST, CIFAR10, and TinyImagenet datasets with and without GP operations.

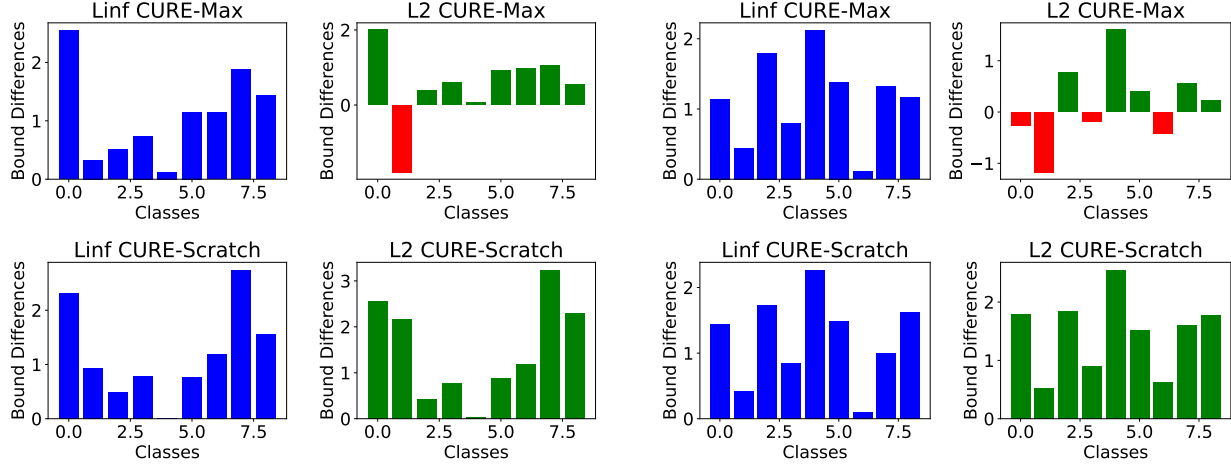


Figure 8: Bound difference visualizations on CIFAR-10 ( $\epsilon_\infty = \frac{8}{255}, \epsilon_2 = 0.5$ ) experiments.

We see that the GP operation’s cost is small compared with the whole training procedure, accounting for around 6% of the whole training time.

	MNIST	CIFAR-10	TinyImagenet
w/o GP	148	390	952
with GP	154	414	1036

Table 11: Runtime for CURE-Scratch on MNIST, CIFAR10, and TinyImagenet datasets.

## E. Algorithms

In this section, we present the algorithms of **CURE** framework. Algorithm 1 illustrates how to get propagation region for both  $l_2$  and  $l_\infty$  perturbations. Algorithm 2, 3, 4, 5 refer to algorithms of CURE-Joint, CURE-Max, CURE-Random, and CURE-Scratch/Finetune, respectively. Algorithm 6 is the procedure of performing GP after one epoch of natural and certified training (could be any of Algorithm 2, 3, 4, 5).



---

**Algorithm 1** get\_propagation\_region for  $l_\infty$  and  $l_2$  perturbations
 

---

**Require:** Neural network  $f$ , input  $\mathbf{x}$ , label  $t$ , perturbation radius  $\epsilon$ , subselection ratio  $\lambda$ , step size  $\alpha$ , step number  $n$ , attack types  $\in \{l_\infty, l_2\}$

**Ensure:** Center  $\mathbf{x}'$  and radius  $\tau$  of propagation region  $\mathcal{B}^\tau(\mathbf{x}')$

```

 $(\underline{\mathbf{x}}, \overline{\mathbf{x}}) \leftarrow \text{clamp}((\mathbf{x} - \epsilon, \mathbf{x} + \epsilon), 0, 1)$  // Get bounds of input region
 $\tau \leftarrow \lambda/2 \cdot (\overline{\mathbf{x}} - \underline{\mathbf{x}})$  // Compute propagation region size  $\tau$ 
 $\mathbf{x}_0^* \leftarrow \text{Uniform}(\underline{\mathbf{x}}, \overline{\mathbf{x}})$  // Sample PGD initialization
for  $i = 0 \dots n - 1$  do // Do  $n$  PGD steps
    if attack =  $l_\infty$  then // PGD- $l_\infty$ 
         $\mathbf{x}_{i+1}^* \leftarrow \mathbf{x}_i^* + \alpha \cdot \epsilon \cdot \text{sign}(\nabla_{\mathbf{x}_i^*} \mathcal{L}_{\text{CE}}(f(\mathbf{x}_i^*), t))$ 
         $\mathbf{x}_{i+1}^* \leftarrow \text{clamp}(\mathbf{x}_{i+1}^*, \underline{\mathbf{x}}, \overline{\mathbf{x}})$ 
    end if
    if attack =  $l_2$  then // PGD- $l_2$ 
         $\mathbf{x}_{i+1}^* \leftarrow \mathbf{x}_i^* + \alpha \cdot \frac{\nabla_{\mathbf{x}_i^*} \mathcal{L}_{\text{CE}}(f(\mathbf{x}_i^*), \mathbf{y})}{\|\nabla_{\mathbf{x}_i^*} \mathcal{L}_{\text{CE}}(f(\mathbf{x}_i^*), \mathbf{y})\|_2}$ 
         $\delta \leftarrow \frac{\epsilon}{\|\mathbf{x}_{i+1}^* - \mathbf{x}\|_2} \cdot (\mathbf{x}_{i+1}^* - \mathbf{x})$ 
         $\mathbf{x}_{i+1}^* \leftarrow \text{clamp}(\mathbf{x} + \delta, \underline{\mathbf{x}}, \overline{\mathbf{x}})$ 
    end if
end for
 $\mathbf{x}' \leftarrow \text{clamp}(\mathbf{x}_n^*, \underline{\mathbf{x}} + \tau, \overline{\mathbf{x}} - \tau)$  // Ensure that  $\mathcal{B}^\tau(\mathbf{x}')$  will lie fully in  $\mathcal{B}^\epsilon(\mathbf{x})$ 
return  $\mathbf{x}', \tau$ 
    
```

---



---

**Algorithm 2** CURE-Joint Training Epoch
 

---

**Require:** Neural network  $f_\theta$ , training set  $(\mathbf{X}, \mathbf{T})$ , perturbation radius  $\epsilon_2$  and  $\epsilon_\infty$ , subselection ratio  $\lambda_\infty$  and  $\lambda_2$ , learning rate  $\eta$ ,  $\ell_1$  regularization weight  $\ell_1$ , loss balance factor  $\alpha$

```

for  $(\mathbf{x}, t) = (\mathbf{x}_0, t_0) \dots (\mathbf{x}_b, t_b)$  do // Sample batches  $\sim (\mathbf{X}, \mathbf{T})$ 
     $(\mathbf{x}'_\infty, \tau_\infty) \leftarrow \text{get\_propagation\_region}(\text{attack} = l_\infty)$  // Refer to Algorithm 1
     $(\mathbf{x}'_2, \tau_2) \leftarrow \text{get\_propagation\_region}(\text{attack} = l_2)$ 
     $\mathcal{B}^{\tau_\infty}(\mathbf{x}'_\infty) \leftarrow \text{BOX}(\mathbf{x}'_\infty, \tau_\infty)$  // Get box with midpoint  $\mathbf{x}'_\infty, \mathbf{x}'_2$  and radius  $\tau_\infty, \tau_2$ 
     $\mathcal{B}^{\tau_2}(\mathbf{x}'_2) \leftarrow \text{BOX}(\mathbf{x}'_2, \tau_2)$ 
     $\mathbf{u}_{y_\infty}^\Delta \leftarrow \text{get\_upper\_bound}(f_\theta, \mathcal{B}^{\tau_\infty}(\mathbf{x}'_\infty))$  // Get upper bound  $\mathbf{u}_{y_\infty}^\Delta, \mathbf{u}_{y_2}^\Delta$  on logit differences
     $\mathbf{u}_{y_2}^\Delta \leftarrow \text{get\_upper\_bound}(f_\theta, \mathcal{B}^{\tau_2}(\mathbf{x}'_2))$  // based on IBP
     $\text{loss}_{l_\infty} \leftarrow \mathcal{L}_{\text{CE}}(\mathbf{u}_{y_\infty}^\Delta, t)$ 
     $\text{loss}_{l_2} \leftarrow \mathcal{L}_{\text{CE}}(\mathbf{u}_{y_2}^\Delta, t)$ 
     $\text{loss}_{\ell_1} \leftarrow \ell_1 \cdot \text{get\_}\ell_1\text{-norm}(f_\theta)$ 
     $\text{loss}_{\text{tot}} \leftarrow (1 - \alpha) \cdot \text{loss}_{l_\infty} + \alpha \cdot \text{loss}_{l_2} + \text{loss}_{\ell_1}$ 
     $\theta \leftarrow \theta - \eta \cdot \nabla_\theta \text{loss}_{\text{tot}}$  // Update model parameters  $\theta$ 
end for
    
```

---

**Algorithm 3** CURE-Max Training Epoch

---

**Require:** Neural network  $f_\theta$ , training set  $(\mathbf{X}, \mathbf{T})$ , perturbation radius  $\epsilon_2$  and  $\epsilon_\infty$ , subselection ratio  $\lambda_\infty$  and  $\lambda_2$ , learning rate  $\eta$ ,  $\ell_1$  regularization weight  $\ell_1$

**for**  $(\mathbf{x}, t) = (\mathbf{x}_0, t_0) \dots (\mathbf{x}_b, t_b)$  **do** // Sample batches  $\sim (\mathbf{X}, \mathbf{T})$

$(\mathbf{x}'_\infty, \tau_\infty) \leftarrow \text{get\_propagation\_region}(\text{attack} = l_\infty)$  // Refer to Algorithm 1

$(\mathbf{x}'_2, \tau_2) \leftarrow \text{get\_propagation\_region}(\text{attack} = l_2)$

$\mathcal{B}^{\tau_\infty}(\mathbf{x}'_\infty) \leftarrow \text{BOX}(\mathbf{x}'_\infty, \tau_\infty)$  // Get box with midpoint  $\mathbf{x}'_\infty, \mathbf{x}'_2$  and radius  $\tau_\infty, \tau_2$

$\mathcal{B}^{\tau_2}(\mathbf{x}'_2) \leftarrow \text{BOX}(\mathbf{x}'_2, \tau_2)$

$\mathbf{u}_{y_\infty}^\Delta \leftarrow \text{get\_upper\_bound}(f_\theta, \mathcal{B}^{\tau_\infty}(\mathbf{x}'_\infty))$  // Get upper bound  $\mathbf{u}_{y_\infty}^\Delta, \mathbf{u}_{y_2}^\Delta$  on logit differences

$\mathbf{u}_{y_2}^\Delta \leftarrow \text{get\_upper\_bound}(f_\theta, \mathcal{B}^{\tau_2}(\mathbf{x}'_2))$  // based on IBP

$\text{loss}_{l_\infty} \leftarrow \mathcal{L}_{\text{CE}}(\mathbf{u}_{y_\infty}^\Delta, t)$

$\text{loss}_{l_2} \leftarrow \mathcal{L}_{\text{CE}}(\mathbf{u}_{y_2}^\Delta, t)$

$\text{loss}_{\text{Max}} \leftarrow \max(\text{loss}_{l_\infty}, \text{loss}_{l_2})$  // We select the largest  $l_{p \in [2, \infty]}$  loss for each sample

$\text{loss}_{\ell_1} \leftarrow \ell_1 \cdot \text{get\_}\ell_1\text{-norm}(f_\theta)$

$\text{loss}_{\text{tot}} \leftarrow \text{loss}_{\text{Max}} + \text{loss}_{\ell_1}$

$\theta \leftarrow \theta - \eta \cdot \nabla_\theta \text{loss}_{\text{tot}}$  // Update model parameters  $\theta$

**end for**

---

**Algorithm 4** CURE-Random Training Epoch

---

**Require:** Neural network  $f_\theta$ , training set  $(\mathbf{X}, \mathbf{T})$ , perturbation radius  $\epsilon_2$  and  $\epsilon_\infty$ , subselection ratio  $\lambda_\infty$  and  $\lambda_2$ , learning rate  $\eta$ ,  $\ell_1$  regularization weight  $\ell_1$

**for**  $(\mathbf{x}, t) = (\mathbf{x}_0, t_0) \dots (\mathbf{x}_b, t_b)$  **do** // Sample batches  $\sim (\mathbf{X}, \mathbf{T})$

$(\mathbf{x}_1, \mathbf{x}_2), (t_1, t_2) \leftarrow \text{partition}(\mathbf{x}, t)$  // Randomly partition inputs into two blocks

    // Apply Algorithm 1

$(\mathbf{x}'_\infty, \tau_\infty) \leftarrow \text{get\_propagation\_region}(\mathbf{x}_1, t_1, \text{attack} = l_\infty)$

$(\mathbf{x}'_2, \tau_2) \leftarrow \text{get\_propagation\_region}(\mathbf{x}_2, t_2, \text{attack} = l_2)$

$\mathcal{B}^{\tau_\infty}(\mathbf{x}'_\infty) \leftarrow \text{BOX}(\mathbf{x}'_\infty, \tau_\infty)$  // Get box with midpoint  $\mathbf{x}'_\infty, \mathbf{x}'_2$  and radius  $\tau_\infty, \tau_2$

$\mathcal{B}^{\tau_2}(\mathbf{x}'_2) \leftarrow \text{BOX}(\mathbf{x}'_2, \tau_2)$

$\mathbf{u}_{y_\infty}^\Delta \leftarrow \text{get\_upper\_bound}(f_\theta, \mathcal{B}^{\tau_\infty}(\mathbf{x}'_\infty))$  // Get upper bound  $\mathbf{u}_{y_\infty}^\Delta, \mathbf{u}_{y_2}^\Delta$  on logit differences

$\mathbf{u}_{y_2}^\Delta \leftarrow \text{get\_upper\_bound}(f_\theta, \mathcal{B}^{\tau_2}(\mathbf{x}'_2))$  // based on IBP

$\text{loss}_{l_\infty} \leftarrow \mathcal{L}_{\text{CE}}(\mathbf{u}_{y_\infty}^\Delta, t)$

$\text{loss}_{l_2} \leftarrow \mathcal{L}_{\text{CE}}(\mathbf{u}_{y_2}^\Delta, t)$

$\text{loss}_{\ell_1} \leftarrow \ell_1 \cdot \text{get\_}\ell_1\text{-norm}(f_\theta)$

$\text{loss}_{\text{tot}} \leftarrow \text{loss}_{l_\infty} + \text{loss}_{l_2} + \text{loss}_{\ell_1}$

$\theta \leftarrow \theta - \eta \cdot \nabla_\theta \text{loss}_{\text{tot}}$  // Update model parameters  $\theta$

**end for**

---

---

**Algorithm 5** CURE-Scratch/Finetune Training Epoch

**Require:** Neural network  $f_\theta$ , training set  $(\mathbf{X}, \mathbf{T})$ , perturbation radius  $\epsilon_2$  and  $\epsilon_\infty$ , subselection ratio  $\lambda_\infty$  and  $\lambda_2$ , learning rate  $\eta$ ,  $\ell_1$  regularization weight  $\ell_1$ , KL loss balance factor  $\eta$ , mode  $\in [\text{Scratch}, \text{Finetune}]$   
**for**  $(\mathbf{x}, t) = (\mathbf{x}_0, t_0) \dots (\mathbf{x}_b, t_b)$  **do** // Sample batches  $\sim (\mathbf{X}, \mathbf{T})$   
      $(\mathbf{x}'_\infty, \tau_\infty) \leftarrow \text{get\_propagation\_region}(\text{attack} = l_\infty)$  // Refer to Algorithm 1  
      $(\mathbf{x}'_2, \tau_2) \leftarrow \text{get\_propagation\_region}(\text{attack} = l_2)$   
      $\mathcal{B}^{\tau_\infty}(\mathbf{x}'_\infty) \leftarrow \text{BOX}(\mathbf{x}'_\infty, \tau_\infty)$  // Get box with midpoint  $\mathbf{x}'_\infty, \mathbf{x}'_2$  and radius  $\tau_\infty, \tau_2$   
      $\mathcal{B}^{\tau_2}(\mathbf{x}'_2) \leftarrow \text{BOX}(\mathbf{x}'_2, \tau_2)$   
      $\mathbf{u}_{y_\infty}^\Delta \leftarrow \text{get\_upper\_bound}(f_\theta, \mathcal{B}^{\tau_\infty}(\mathbf{x}'_\infty))$  // Get upper bound  $\mathbf{u}_{y_\infty}^\Delta, \mathbf{u}_{y_2}^\Delta$  on logit differences  
      $\mathbf{u}_{y_2}^\Delta \leftarrow \text{get\_upper\_bound}(f_\theta, \mathcal{B}^{\tau_2}(\mathbf{x}'_2))$  // based on IBP  
      $\text{loss}_{l_\infty} \leftarrow \mathcal{L}_{\text{CE}}(\mathbf{u}_{y_\infty}^\Delta, t)$   
      $\text{loss}_{l_2} \leftarrow \mathcal{L}_{\text{CE}}(\mathbf{u}_{y_2}^\Delta, t)$   
      $\text{loss}_{\text{Max}} \leftarrow \max(\text{loss}_{l_\infty}, \text{loss}_{l_2})$  // We select the largest  $l_{p \in [2, \infty]}$  loss for each sample  
      $\text{loss}_{\ell_1} \leftarrow \ell_1 \cdot \text{get\_}\ell_1\text{-norm}(f_\theta)$   
     find correctly certified  $l_q$  subset  $\gamma$  using Definition 4.3  
      $\text{loss}_{KL} \leftarrow KL(d_q[\gamma] || d_r[\gamma])$  // Eq. 5  
      $\text{loss}_{\text{tot}} \leftarrow \text{loss}_{\text{Max}} + \eta \cdot \text{loss}_{KL} + \text{loss}_{\ell_1}$   
      $\theta \leftarrow \theta - \eta \cdot \nabla_\theta \text{loss}_{\text{tot}}$  // Update model parameters  $\theta$   
**end for**

---



---

**Algorithm 6** GP: Connect CT with NT

1: **Input:** model  $f_\theta$ , input images with distribution  $\mathcal{D}$ , training rounds  $R$ ,  $\beta$ , natural training **NT** and certified training **CT** algorithms, perturbation radius  $\epsilon_\infty$  and  $\epsilon_2$ , subselection ratio  $\lambda_\infty$  and  $\lambda_2$ , learning rate  $\eta$ ,  $\ell_1$  regularization weight  $\ell_1$ .  
 2:  
 3: **for**  $r = 1, 2, \dots, R$  **do**  
 4:    $f_n \leftarrow \text{NT}(f_\theta^{(r)}, \mathcal{D})$   
 5:    $f_c \leftarrow \text{CT}(f_\theta^{(r)}, \epsilon_\infty, \epsilon_2, \lambda_\infty, \lambda_2, \eta, \ell_1, \mathcal{D})$  // Can be single-norm or any CURE training  
 6:   compute  $g_n \leftarrow f_n - f_\theta^{(r)}$ ,  $g_c \leftarrow f_c - f_\theta^{(r)}$   
 7:   compute  $g_p$  using Eq. 10  
 8:   update  $f_\theta^{(r+1)}$  using Eq. 11 with  $\beta$  and  $g_c$   
 9: **end for**  
 10: **Output:** model  $f_\theta$ .

---